Journal of Hazardous Materials, Volume 480, December 2024, Article number 135908
DOI: 10.1016/j.jhazmat.2024.135908

Comprehensive geophysical, geotechnical, and geochemical assessments of an offshore landfill in Singapore

Zhibo Zhang[a], Ziwen Yuan[a], Lei Hu[a], Frederic Coulon[b], Huaxin Liu[a], Zhanbo Cheng[a], Shifan Wu[a], Qian Liu[ac], Xiaoqing Pi[a], Wei Wu[a], Xunchang Fei[ac*]

[a] School of Civil and Environmental Engineering, Nanyang Technological University, 50 Nanyang Ave, 639798, Singapore

[b] School of Water, Energy, and Environment, Cranfield University, Cranfield, MK43 0AL, UK

[c] Residues and Resource Reclamation Centre, Nanyang Environment and Water Research Institute, 1 Cleantech Loop, 637141, Singapore

[*] Corresponding author: Xunchang Fei

Email address: xcfei@ntu.edu.sg

Postal address: N1 building 01C-70, School of Civil and Environmental Engineering, Nanyang Technological University, 50 Nanyang Ave, 639798, Singapore

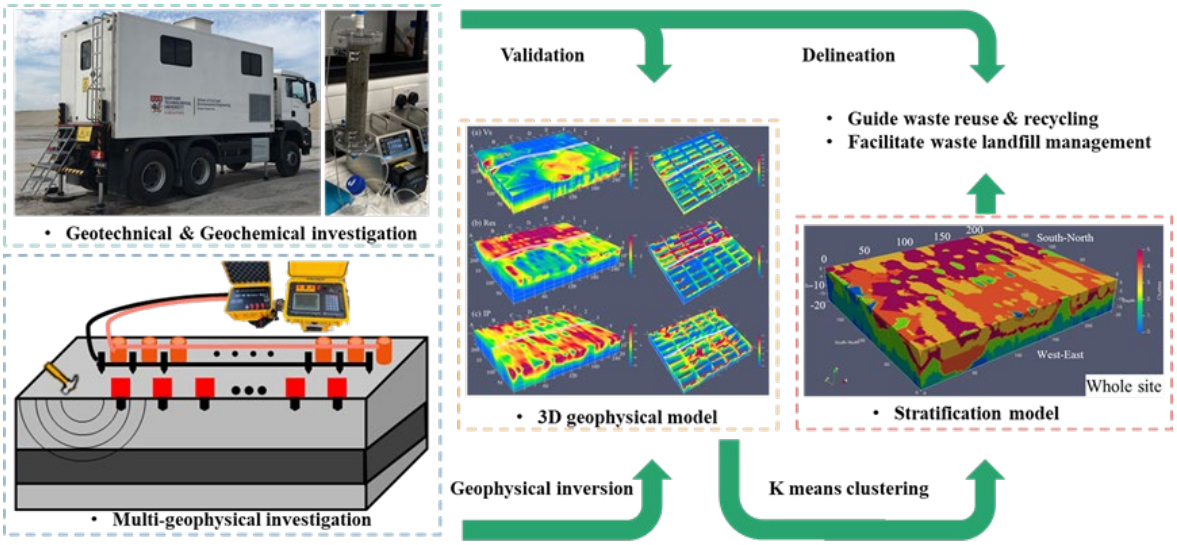
Published by Elsevier. This is the Author Accepted Manuscript issued with: Creative Commons Attribution License (CC:BY 4.0).
The final published version (version of record) is available online at DOI:10.1016/j.jhazmat.2024.135908. Please refer to any applicable publisher terms of use.

Highlights

- Geophysical site investigation supplemented with geotechnical and geochemical data.
- Delineation of waste-clay boundary and potential leachate leakage detection.
- Identification and quantification of waste materials and recoverable metals.
- A machine learning-based 3D model for an offshore landfill.

10

Graphic abstract



11

Abstract

Comprehensive site investigation techniques, including Electrical Resistivity Tomography (ERT), Induced Polarization (IP), Multichannel Analysis of Surface Waves (MASW), and Microtremor Array Method (MAM), were integrated with geotechnical and geochemical tests of retrieved waste samples from Singapore's operational offshore landfill. The properties of landfill wastes vary widely, including shear-wave velocities 127-248 m/s, densities 1.2-2.1 Mg/m^3, resistivity 3.0-25.3 Ω·m, and chargeability 48-82 mV/V. The natural clay layer underneath was clearly delineated and effectively mitigated leachate leakage. K-means clustering of the geophysical data facilitates precise mapping of waste distribution and quantities of recoverable metals based on quantitative criteria. This study illustrates a thorough case study adopting a new site investigation and characterization paradigm for an offshore landfill, which provides insights into leachate leakage detection and evaluations of landfill mining and resource recovery.

Keywords: landfill investigation, electrical resistivity tomography, time-domain induced polarization, shear-wave velocity, 3D geophysical modeling, K-means clustering.

1 Introduction

Over two-thirds of global wastes were disposed in managed and unmanaged landfills, and open dump sites, highlighting a critical environmental challenge (ISWA, 2024; Kaza et al., 2018). Europe alone has over 500,000 sites (Jacobs, 2018; Pi et al., 2023; Vaverková, 2019). To align with the goals of Agenda 21 and Sustainable Development Goal 12: "responsible consumption and production" (SDG 12), there is a growing emphasis on environmentally friendly waste management strategies that prioritize resource recovery and reuse (Fei et al., 2021; Fei et al., 2022;

He et al., 2023; Wei et al., 2024; Zhang et al., 2023). Over the past decade, landfill mining and enhanced landfill mining have emerged as step-change approaches in this context, focusing on extracting valuable materials from existing landfill sites (Jones et al., 2013; Wagland et al., 2019; Zhang et al., 2024). Comprehensive landfill surveys play a vital role in this context, as they provide critical data for waste management and key information for guiding landfill mining, recovery and reuse of valuable materials. While traditional methods such as borehole drilling provide accurate results, they are often costly, time-consuming, labor-intensive, and limited in terms of site coverage or sample depth. As a result, novel methods, especially geophysical methods due to their convenience, cost-effectiveness, extensive coverage, non-invasive testing, and direct correlation with the physicochemical properties of materials, are being increasingly utilized in landfill investigations. (Loke et al., 2013; Pazzi et al., 2019; Zekkos et al., 2014).

Seismic methods such as Spectral Analysis of Surface Waves (SASW), Horizontal-to-Vertical Spectral Ratio (HVSR), Microtremor Array Measurement (MAM), and Multichannel Analysis of Surface Waves (MASW), are often used for exploring geological features. MASW is particularly useful in landfill investigations due to its convenience and high-resolution 2D and 3D spatial data acquisition (Olafsdottir et al., 2018). MAM which captures low-frequency noise signals, allows for deeper subsurface structure characterization. These 2 methods are used to assess the spatial and temporal variation of shear wave velocity (V_s) (Sahadewa et al., 2014a), investigate landfill depths and areas (Abreu et al., 2016; Greenwood et al., 2015), assess landfill consolidation, and evaluate the dynamic properties of wastes (Carpenter et al., 2013; Sahadewa et al., 2014b). Important parameters such as shear modulus can be estimated utilizing V_S derived from MASW and MAM (Zekkos et al., 2008; Zekkos et al., 2014).

Electrical methods, such as electrical resistivity tomography (ERT), are also widely used due to their close correlation with the geochemical properties of waste (Chambers et al., 2006; Gabarrón et al., 2020; Soupios et al., 2007). ERT has also evolved enabling 2D and 3D investigation, and time-lapse monitoring (Loke et al., 2013). ERT is commonly used to assess the extent and depth of landfill sites, estimate the moisture content, and evaluate the impact of landfill leachate on surrounding environmental water sources (Clément et al., 2010; Pomposiello et al., 2012). Induced Polarization (IP) is used to ascertain the composition and chemical states of valuable metals within landfills and to identify active biodegradation zones. (Sumner, 2012; Titov et al., 2002).

Given the inherent non-uniqueness of geophysical inversion results a single method is often insufficient to provide a comprehensive characterization of landfill sites (Dumont et al., 2017). Thus, it is necessary to integrate multiple geophysical methods to enhance site resolution and provide a comprehensive characterization of sites. For example, studies have shown that joint inversion of electrical resistivity and seismic refraction data (Steiner et al., 2022), as well as combining electromagnetic (EM) and ERT methods, can effectively assess landfill conditions, landfill consolidation and leachate distribution and metallic hotspot presence (Di Maio et al., 2018).

It is also advisable to complement geophysical approaches with geotechnical investigation and geochemical analysis when investigating landfill sites. For instance, combining ERT and SASW with borehole data (Yin et al., 2015), or integrating IP with geochemical analysis (Manrique et al., 2024), enhances the assessment of metal enrichment in waste sites and helps guide recycling strategies for valuable materials. Advanced statistical methods and machine learning techniques

are also increasingly used to analyze geophysical data, providing more reliable interpretations and objective data classification. This approach is exemplified by studies mapping leachate contamination using ERT and IP results with unsupervised machine learning clustering (Wang et al., 2024).

In this study, a comprehensive field investigation and analysis was carried out for an offshore landfill in Singapore to (1) evaluate the spatial distribution and depth of waste deposits, as well as identify any potential leakage points; (2) develop and validate criteria for stratifying different waste layers using geophysical, geotechnical, and geochemical methods; (3) implement unsupervised machine learning techniques to analyze geophysical inversion results for better stratification and zoning of geological layers within the landfill, and (4) perform statistical analyses to characterize the differences and ranges of geophysical parameters across various waste layers. To the best of the author's knowledge, this is the most comprehensive characterization study of an offshore landfill, assessing both waste materials and the potential for resource recovery and reuse.

2 Methodologies

The overall methodological approach used is presented in Fig. 1. The solid black boundary lines and the dashed red boundary lines delineate the primary steps of the traditional methods and the innovative approach proposed in this study, respectively. Both approaches involve thorough site investigation using established geophysical detection methods, alongside processes like filtering, noise reduction, and inversion calculations of raw data. For the traditional analysis, inversion results and expert judgment are used to determine soil layer interfaces, typically analyzing different geophysical parameters independently. In contrast, our comprehensive site investigation

approach employs machine learning to objectively cluster sites based on geophysical inversion results. This approach provides clear, quantitative criteria for delineating waste and soil layers, offering spatial distribution estimates. Geotechnical and geochemical information is used to validate the clustering results, correlating them with the actual stratigraphy and offering interpretations of their practical meanings.

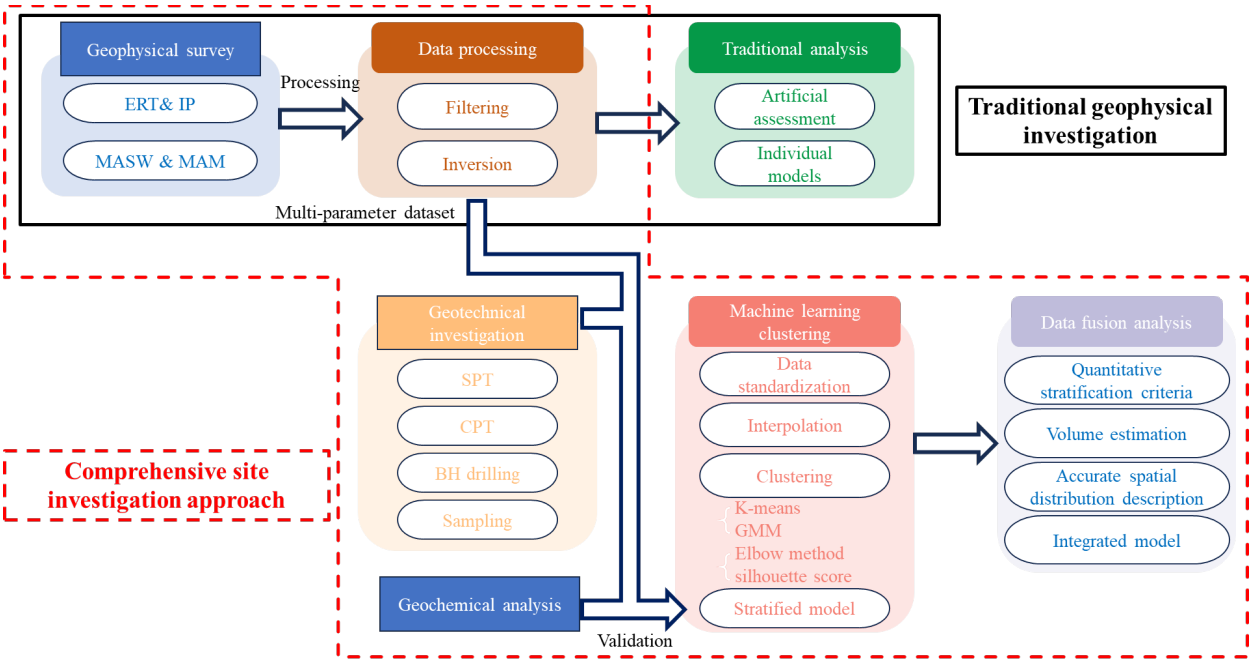


Fig. 1. Comparison of the traditional geophysical investigation approach and the comprehensive site investigation approach used in this study.

2.1 Site description

The offshore landfill is an artificial island which was reclaimed from shoals and surrounded by a rock bund with impermeable geomembranes and marine clay layers to prevent the leakage of inside water and leachate. The top of the waste materials was covered by a layer of soil encroached by spontaneous vegetation without geomembrane, as shown in Fig. 2 and Fig. 5a. At the bottom of the landfill, seabed sediments prevent pollution from seeping out.

The original seabed consists primarily of clay from the Kallang Formation (KF), interspaced with silty sand and silt layers, underlay by weathered rock layers from the Jurong Formation (JF). The KF is typically 8-12 meters thick, with localized deposits of 1-2 m layer of silty sand and silt (F1 layer). The landfill experiences tropical weather conditions, with temperatures ranging from 23 to 34 ℃, humidity levels between 65% to 90%, and an average annual rainfall of about 2,400 mm, concentrated mostly between November and March. Cell N and S were first used for waste disposal, covering 12.4 and 12.6 hectares respectively. A 6-meter-wide internal road atop a compacted soil embankment separates these two cells, each capped with 0.3-0.5 meters of natural soil (Fig. 2).

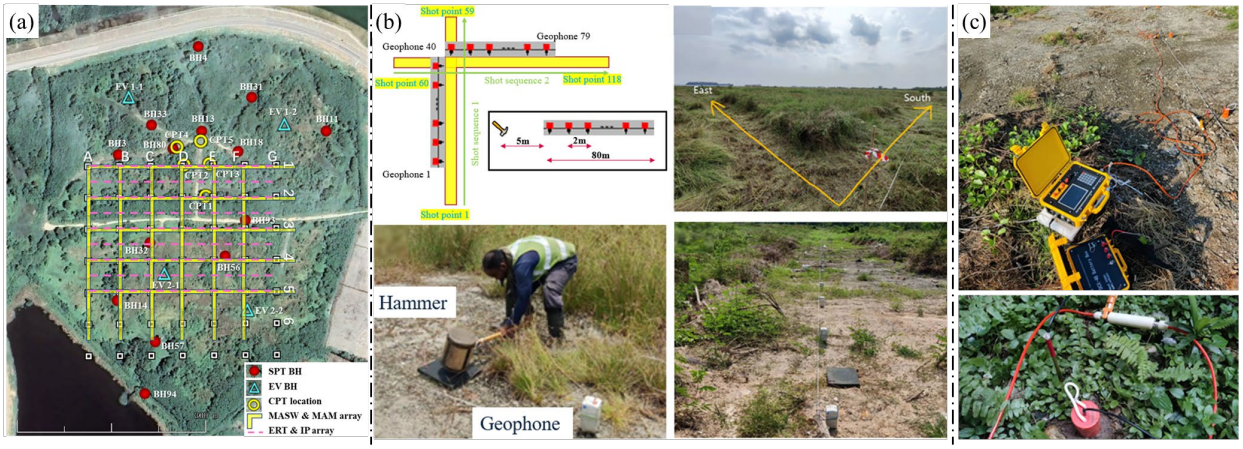


Fig. 2. Site information and geophysical investigation setup: (a) geophysical investigation plan and test locations; (b) MASW and MAM equipment; (c) ERT and IP equipment.

2.2 Geotechnical site investigation and chemical analysis of samples

16 SPT boreholes (BH) and 4 Environmental boreholes (EV BH) were strategically located to cover both Cell N and S. SPT BHs were drilled to depths ranging from 20 to 30 m to penetrate through the waste layer, KF, and conduct at least 2 SPTs in the JF. Below a depth of 1.5 m, SPT was performed every 3 m, and soil samples were taken between two SPT tests to minimize

disturbance. During testing, information such as the appearance and density of waste and soil layers was recorded in the borelogs.

EV BHs allow to obtain samples from the waste layer at different depths, as well as the clay layer below to determine if leachate infiltration had occurred. Undisturbed soil samples were obtained during the drilling process using a thin-wall tube sampler with a diameter of 70 mm. Samples were taken from depths of 0.5-1 m, 2-3 m, 8-9 m, and 12-13 m. After drilling, the PVC tubes were installed to set up monitoring wells, and the area around the wellhead was sealed with bentonite. Water samples were collected from 2 meters below the groundwater level (bgl). The collected solid and liquid samples were well packaged and stored in a 4 °C cold storage room before testing. Solid samples were characterized according to EPA method 3051A (EPA, 2007) and 6010D (EPA, 2014). Briefly, the solid samples were digested by nitric acid or mixed acids of nitric acid and hydrochloric acid, with the aid of microwave heating. The digested samples were then analyzed to determine their heavy metal contents. The heavy metals in the water samples were also measured according to APHA method 3120B, 3125B, 3112B (APHA, 2017a, b, c). The test results were compared with the intervention values (IV) recommended by the "Soil Remediation Circular" (2013) as required by Jurong Town Corporation in Singapore, to determine if the elements and compounds exceeded the standard limits.

CPT was mainly conducted near the geophysical survey lines in Cell N for comparison and validation purposes (Fig. 2a). The tests were performed using the Geomil GEM3 CPT truck according to ASTM (2016). The cone penetrated through the waste layer and stopped at a depth of 20 m. The thickness of the waste layer and clay layer was determined based on the measured

tip resistance (q_t), sleeve friction (f_s), and water pressure (u_0) values (Kou et al., 2016; Wang, H. et al., 2021).

2.3 Geophysical site investigation

The site investigation was conducted on the 250 m × 250 m test area depicted in Fig. 2a, spanning across Cell N and Cell S. The site was divided into 6 rows labeled A to F along the west-east (WE) direction and numbered 1 to 7 along the north-south (NS) direction, with coordinates for lines 6-7 provided for hammering during MASW testing. ERT and IP tests were conducted in 9 lines with 250 m length along the NS direction at 25 m intervals. As the MAM test requires natural noise from all directions, an L-shaped array (Fig. 2c) was engaged to fulfill the requirement of both MASW and MAM tests. Seismic wave was generated for MASW tests using a 15 kg sledgehammer and a rubber plate 5 m away from the first geophone to allow for full development of surface waves. Each array has two side wings with 80 m length, in which geophones were arranged at 2 m intervals. 30 MASW and 30 MAM tests were completed in 5 rows and 6 columns, with 50 m intervals in each direction. 3 shots were made at each test point, and their wave records were superimposed to suppress noise interference and enhance data quality. A GPS device was used to record the accurate triggering timepoint. After each MASW test, all geophones were left in place for one hour to record the surrounding ambient noise for the MAM test.

For ERT and IP testing, a DUK8 direct current instrument from the China Geological Group was used, as shown in Fig. 2b with the instrument connected to five 50 m-long cables. At every 5 m interval along the cable, a copper rod electrode and a non-polarizable electrode were connected for measuring current and voltage, respectively. This electrode spacing was chosen based on a

197 comprehensive evaluation of efficiency, resolution, site conditions, and the recommendations for
198 environmental surveys by M.H.Loke (2022). Standard metal electrodes exhibit noticeable self-
199 polarization when energized, which can affect the precise measurement of weak secondary fields
200 in IP testing (Abdulsamad et al., 2016). Hence non-polarizable electrodes were utilized.
201 Considering the site conditions and the results of trial tests, a Wenner array was employed. At each
202 measurement point, tests were repeated twice to ensure the accuracy and stability of the data.
203 During each measurement, the current was turned on for 2 seconds to measure stable resistance,
204 followed by a 1-second power-off period to capture the attenuation process of secondary fields
205 using non-polarizable electrodes, yielding IP data.
206
207 **2.4 Processing and analysis of geophysical data**
208 The initial ERT and IP test results were filtered based on sensitivity values and repeated test errors
209 to remove outliers and anomalies. The processed ERT/IP data from each survey line were
210 combined into a 3D dataset and imported into RES3D software for inversion. A refined grid was
211 used to achieve the desired data density. The inversion process relied on the initial forward model,
212 using a Gauss-Newton iterative formulation for apparent resistivity inversion (Loke and Barker,
213 1996), and a linear approximation method for apparent IP inversion (Oldenburg and Li, 1994). The
214 final inversion model was converged by iteratively minimizing the difference between the
215 inversion model and the true results with the least squares method. For the MASW data, the shear-
216 wave records were first extracted based on trigger records, and repeated test data were stacked.
217 Frequency filtering was applied to enhance signal quality. The processed data were then integrated
218 according to the on-site geophone layout and imported into Surface Pro software produced by
219 Geogiga Corp. for inversion. The F-V method was used to obtain dispersion curves, followed by

inversion using the genetic method, aiming to converge to the optimal model by minimizing the sum of squared errors (SSE). For MAM, the raw record was cut into small pieces with a 2 min time length, and those with strong low-frequency signals were selected to conduct the inversion calculation based on the Spatial autocorrelation method (Aki, 1957). The dispersion curves extracted from MASW and MAM at the same location were merged for subsequent inversion calculations to achieve better resolution for both shallow and deep layers (Zekkos et al., 2013). All the merged dispersion curves were integrated for inversion to ensure overall convergence. Linear interpolation was applied to fill in missing values, enabling the generation of 3D models for each geophysical parameter. This process ensured consistent spatial coverage and achieved a modeling accuracy of 2 m in the horizontal direction and 1 m in the depth direction. All interpolated data were merged and imported into ParaView software to generate a 3D geophysical model, allowing for the description of spatial distribution and volume estimation of various soil and waste categories.

Due to the site's distinctive characteristics and the scarcity of comparable data from other sites, various unsupervised machine learning methods were attempted to cluster the geophysical inversion results and explore the spatial distribution of different types of waste, in which K-means clustering (KMC) was ultimately selected for its superior silhouette score and low sum of squared error (SSE). KMC aims to partition a dataset into K distinct and non-overlapping clusters (Lloyd, 1982). Each cluster is defined by its centroid μ_i, which is the mean of the points in the cluster. The objective is to minimize the SSE between the points and their respective cluster centroids. KMC begins with the random selection of centroids μ_i. All data points are then assigned to the cluster corresponding to the nearest centroid μ_i. During each iteration, the centroid of each cluster is

243 rearranged as the mean of the points assigned to it. The SSE between the data points and the
244 cluster's centroids is computed using Equation 1.

245 $$J = \sum_{i=1}^{k} \sum_{x \in C_i} \|x - \mu_i\|^2 \quad (1)$$

246 where C_i is the set of points in cluster i, and || || denotes the Euclidean distance.

247

248 These steps are repeated until the centroids no longer change or a maximum number of iterations
249 is reached. The optimal value of K (4-6) is determined using the elbow method (Bholowalia and
250 Kumar, 2014), where the chosen K is the point at which adding another cluster does not
251 significantly reduce the SSE, meaning the reduction is much less than that achieved by adding the
252 previous cluster. Additionally, the prior information about the geology of the landfill was also
253 considered in the selection of K, which ultimately turns out that the optimum value is 6. The
254 clustering analysis in this study was performed using the Scikit-learn library in Python 3.0.

255

256 **3 Results and discussion**

257 **3.1 Geotechnical analysis and waste characterization**

258 To investigate the distribution of leachate in the landfill, analyze the differences in the waste
259 composition across different areas, and evaluate the effectiveness of underlying clay in preventing
260 pollutant leakage, geochemical analysis was conducted on 16 soil samples and 4 water samples
261 obtained from 4 EV BHs located in different areas. The testing results of solid and liquid samples
262 are summarized in Tables 1, 2 and 3. Metal elements such as cadmium, chromium, copper, lead,
263 nickel, and zinc generally exceeded the standard limits for all the waste samples from both cells.
264 Antimony, barium, cobalt, and molybdenum were found in trace amounts below IVs. Elevated

levels of arsenic and mercury were observed in shallow samples from EV-N-1 BH, potentially due to localized variations in waste composition near that area, although mercury levels overall were minimal throughout the landfill. Horizontal distribution analysis revealed higher concentrations of metal elements in waste samples from the eastern side (EV-N-2 and EV-S-2) compared to the western side (EV-N-1 and EV-S-1).

Metal concentrations in all the clay samples were significantly lower than those in shallower waste samples within the same borehole and below IVs, indicating the effectiveness of clay in preventing leachate leakage. Metal concentrations in the shallow clay samples were generally higher than those in deeper samples, suggesting that leachate may diffuse into the surface clay layer in contact with waste to a limited extent. However, due to the low permeability of clay and the high specific surface area of particles, metal elements are unlikely to migrate into deeper natural soils (Cuevas et al., 2012). Overall, metal element concentrations, except for copper, were higher in Cell S compared to Cell N across all waste and clay samples, indicating greater contamination in Cell S. This disparity may be attributed to groundwater and leachate flow primarily from north to south, directing more metal elements towards Cell S, where waste management practices and landfill duration differences also play contributing roles (Fei and Zekkos, 2018; Fei et al., 2016; He and Fei, 2020).

Table 1. Geochemical results of the waste samples from Cell N

Sample Location	EV-N-1				EV-N-2				Soil Remediation Circular 2013	LOR
Sample type	Waste		Clay		Waste		Clay			
Sample depth	0.5-1 m	2-3 m	8-9 m	12-13 m	0.5-1 m	2-3 m	8-9 m	12-13 m	Intervention Value	-
Metals and Metalloids by US EPA Method 3051A /6010D (Unit mg/kg)										

Arsenic (As)	29	80	13	8	26	20	4	N.D.	76	1.20
Antimony (Sb)	12	8	N.D.	N.D.	7	6	N.D.	N.D.	22	1.20
Barium (Ba)	823	834	11	5	922	745	12	5	-	0.02
Cadmium (Cd)	23	22	1	2	29	29	1	5	13	0.06
Chromium (Cr) Total	165	214	N.D.	N.D.	169	140	N.D.	N.D.	78	78.00
Cobalt (Co)	12	14	3	1	16	14	3	1	190	0.15
Copper (Cu)	1,400	4,135	28	6	3,390	6,661	16	8	190	0.10
Mercury (Hg) Total	4	N.D.	N.D.	N.D.	N.D.	N.D.	N.D.	N.D.	4	4.00
Lead (Pb)	1,847	1,015	18	12	1,756	1,550	13	18	530	0.75
Molybdenum (Mo)	16	48	14	N.D.	24	18	N.D.	N.D.	190	0.15
Nickel (Ni)	150	205	8	2	185	236	7	2	100	0.30
Zinc (Zn)	10,531	5,993	64	20	10,889	6,832	51	34	720	0.10

285

286 **Table 2.** Geochemical results of the waste samples from Cell S

Sample Location	EV-S-1				EV-S-2				Soil Remediation Circular 2013	LOR
Sample type	Waste		Clay		Waste		Clay			
Sample depth	0.5-1 m	2-3 m	8-9 m	12-13 m	0.5-1 m	2-3 m	8-9 m	12-13 m	Intervention Value	-
Arsenic (As)	28	26	7	4	45	34	6	10	76	1.20
Antimony (Sb)	8	9	N.D.	N.D.	8	6	N.D.	N.D.	22	1.20
Barium (Ba)	1,041	678	13	7	991	865	8	9	-	0.02
Cadmium (Cd)	41	30	2	1	43	23	1	2	13	0.06
Chromium (Cr) Total	320	170	N.D.	N.D.	257	216	N.D.	N.D.	78	78.00
Cobalt (Co)	21	14	4	2	29	20	3	4	190	0.15
Copper (Cu)	2,504	3,228	37	20	4,722	4,008	12	84	190	0.10
Mercury (Hg) Total	N.D.	N.D.	N.D.	N.D.	N.D.	N.D.	N.D.	N.D.	4	4.00
Lead (Pb)	2,104	1,573	26	20	2,315	1,236	15	21	530	0.75
Molybdenum (Mo)	25	23	N.D.	0	73	71	0	4	190	0.15
Nickel (Ni)	263	164	8	5	229	205	6	8	100	0.30
Zinc (Zn)	10,671	10,463	112	60	14,204	6,610	39	43	720	0.10

287

Liquid samples were collected from 2 m bgl at each EV BH. Mercury concentrations from all boreholes were above the standard limits, and barium levels except EV-N-1, significantly exceeded the IVs. Other elements remained below the IVs, with some even falling below target values. It is evident that the concentrations of Cd, Cr, Cu, and Pb in the waste far exceed IVs, while these metals are nearly undetectable in the liquid samples. This may be because they primarily exist within the solid components or particles and are unable to encounter groundwater and dissolve. Ni and Zn exceed the standard in the waste but not in the water samples, likely because they predominantly exist in forms that are not readily soluble. In contrast, Ba leaches out more extensively, with its concentration in water samples far exceeding that in solid waste samples. This could be attributed to the higher chloride ion content in the background of the island landfill site, making Ba more prone to dissolution and leaching (Aziz et al., 2017). The concentrations of various elements in the liquid sample are all within the IV range, with some even below the target value. This may be due to nearly 30 years of landfilling and the abundant rainfall in Singapore, which allows most soluble heavy metal pollutants to flow into the wastewater treatment plant reservoir.

Table 3. Geochemical results of the water samples from Cell N and Cell S

Sample Code	EV-N-1	EV-N-2	EV-S-1	EV-S-2	Soil Remediation Circular 2013		LOR
					Target Value	Intervention Value	-
Metals: APHA 23rd Edition 2017: Pt 3120B / 3125B / 3112B (Unit mg/kg)							
Arsenic (As)	N.D.	3.2	1.2	1.4	10.00	60.0	1.00
Antimony (Sb)	5.8	N.D.	N.D.	1.4	-	20.0	1.00
Barium (Ba)	507	2830	1454	1442	50.00	625.0	1.00
Cadmium (Cd)	0.3	0.3	N.D.	N.D.	0.40	6.0	0.25
Chromium (Cr) Total	N.D.	N.D.	N.D.	N.D.	1.00	30.0	30.00
Cobalt (Co)	N.D.	1.2	N.D.	N.D.	20.00	100.0	1.00
Copper (Cu)	10.0	20.3	N.D.	9.3	15.00	75.0	1.50
Mercury (Hg) Total	2.7	2.9	0.8	0.6	0.05	0.3	0.30
Lead (Pb)	N.D.	N.D.	N.D.	N.D.	15.00	75.0	1.50
Molybdenum (Mo)	16.1	4.1	2.7	1.6	5.00	300.0	0.50
Nickel (Ni)	12.0	26.7	3.8	12.9	15.00	75.0	1.50
Zinc (Zn)	90.3	41.8	8.1	108.1	65.00	800.0	1.00

Geotechnical investigations provided key insights into the landfill site characteristics and composition of the waste. Fig. 3 illustrates examples of BH and CPT, in which Fig. 3a and Fig. 3b show CPT and BH outside the geophysical survey area used for cross-validation. Fig. 3c and 3d display CPT results within the geophysical survey area, providing supplementary stratigraphic information for the test area. In BHs, the waste layer composition was confirmed with the collected solid samples. The marine clay layer below the waste was confirmed with SPT N values less than 2. In CPT tests, q_t, f_s, and u_0 were used to confirm the range of the waste layer. Due to the presence of non-incinerable wastes (NIW), household and demolition waste, the q_t and f_s values in this layer are usually higher. In contrast, the clay layer generated excess pore water pressure when the cone passed through due to its lower permeability. When u_0 exceeds the hydrostatic pressure, CPT is considered to have passed through the waste and begun to contact the clay layer. Based on the results of SPT boreholes and CPTs, Fig. 4a displays the distribution of landfill depths. The depths

of waste mainly ranged from 5-9 m. Fig. 4b lists the stratigraphic information of Cell N and S, with Cell S having a higher overall ground elevation than Cell N, higher groundwater levels, and thicker waste layers than Cell N. The groundwater level throughout the cell fluctuated minimally, remaining generally stable within the range of 0-2 m SHD (Singapore height datum). Fig. 5a and 5b show the excavated waste from the site and the waste samples after drying and sieving in the laboratory, respectively. Table 4' shows that those domestic wastes, such as plastic and glass, take a small portion of the total weight while the main components are different size particles, in which large particles (>20mm) mainly come from demolition wastes and smaller particles are mostly incineration ashes, NIW and dust. Fig. 5c and 5d illustrate the significant differences in the appearance of waste between Cell N and Cell S. Samples from Cell N have a lighter color, a higher proportion of particulate materials, and more coarse particles that are more dispersed. These notable differences in appearance indicate significant discrepancies in the waste composition of the two cells. Cell N contains more NIW, inert wastes and construction debris, while Cell S contains more organic matter with higher moisture content and possibly ongoing biological activity. The complex composition of wastes affects leaching behavior (Wang, Q. et al., 2021) and, consequently, influences the electrical responses.

Bulk density generally increases with depth but fluctuates significantly, indicating strong heterogeneity in the waste and the presence of many local weak layers (Fig. 6). The dry density is generally 0.3-0.4 Mg/m^3 lower than the bulk density. The moisture content and saturation vary in both Cells, but the general trends are similar. The specific gravity (G_s) of shallow wastes also fluctuated greatly, mainly due to the complexity of waste components. The G_s of waste materials mainly ranges from 2.5 to 2.7. The void ratio changes dramatically with averaged values ranging

342 from 1.1-1.3 in the waste layer. A substantial decrease begins at the waste-clay interface. Despite
343 the high heterogeneity of the waste leading to significant parameter fluctuations, the average trends
344 of the waste parameters in both cells are similar, with the exception that Cell S has slightly higher
345 G_s and void ratio compared to Cell N.

346

347 **Table 4.** The average composition of the waste in Cell N and Cell S

Content	Plastic	Metal	Yellow soil	Paper	Glass	Ceramics	Rubber	Wood	Particles > 20mm	Particles 10~20mm	Particles <10mm	Total
Ratio (%)	4.6	3.5	3	0.1	1.7	1.1	2.4	0.7	19.8	35.3	27.6	100

348

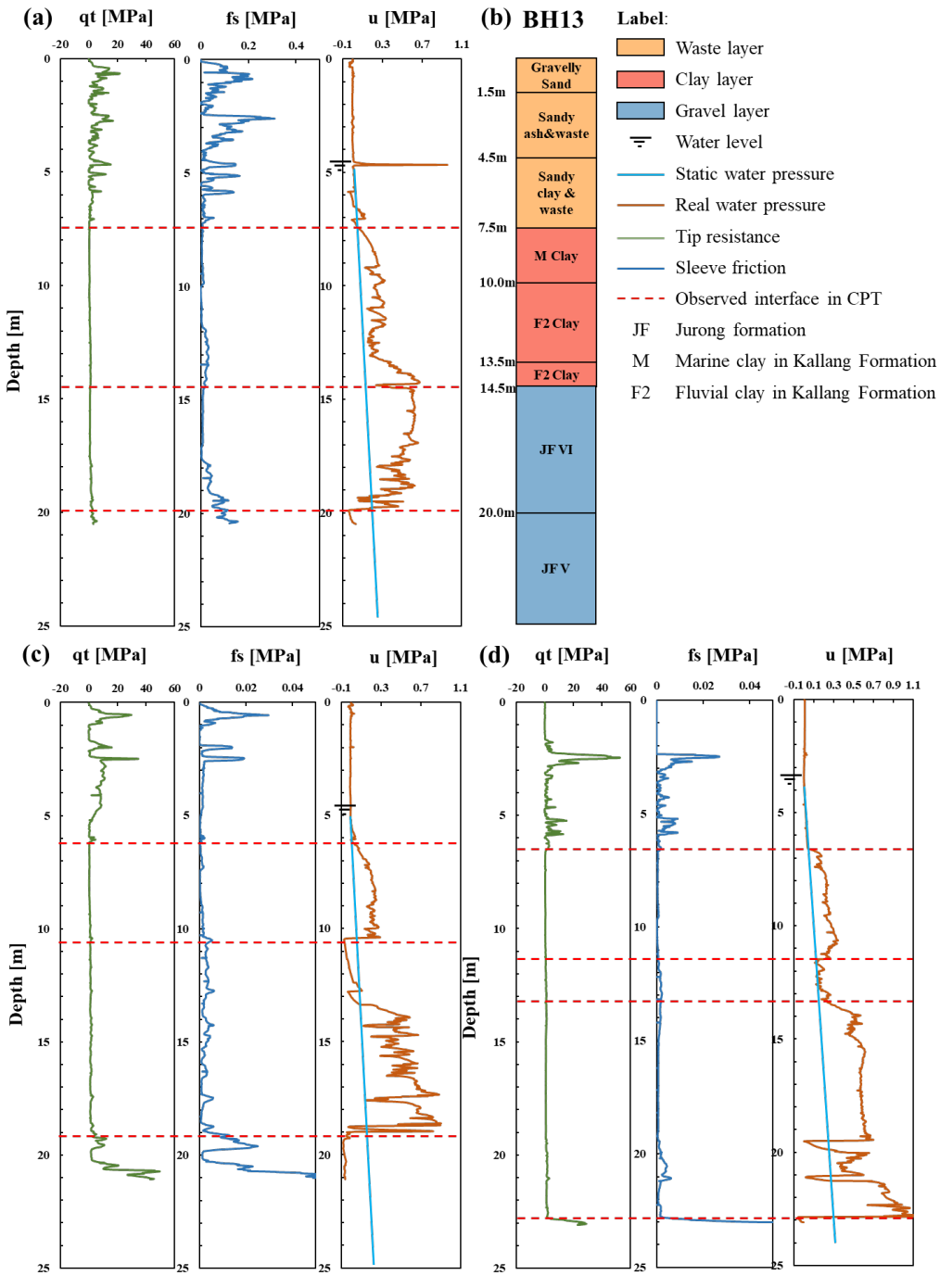
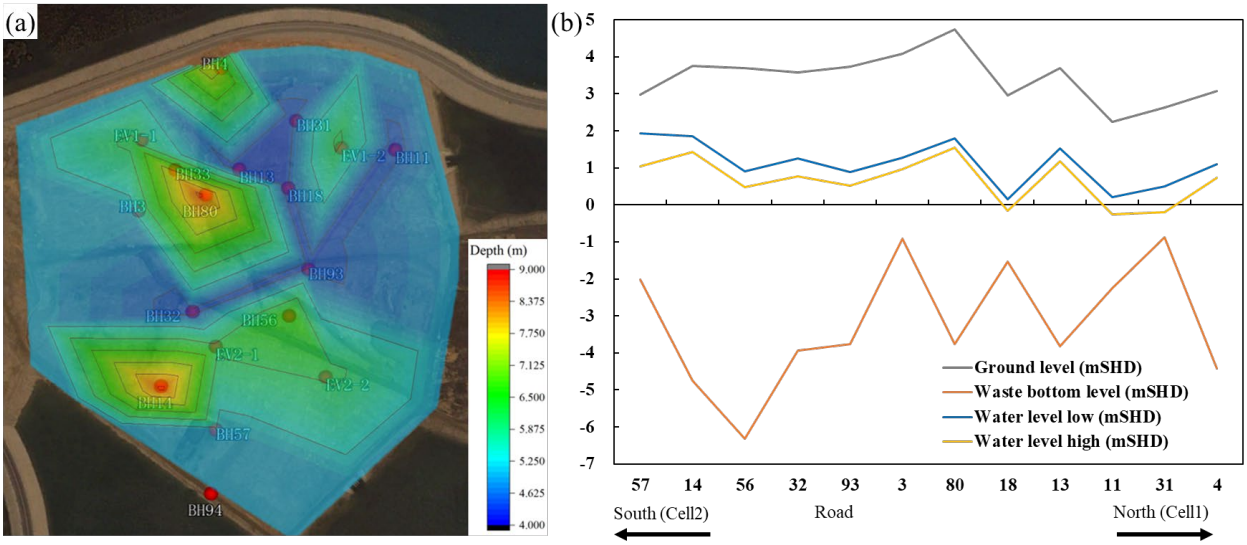


Fig. 3. Examples of SPT and CPT results showing groundwater table and waste-clay interface: (a) CPT 5; (b) BH 13; (c) CPT 1; (d) CPT 2.

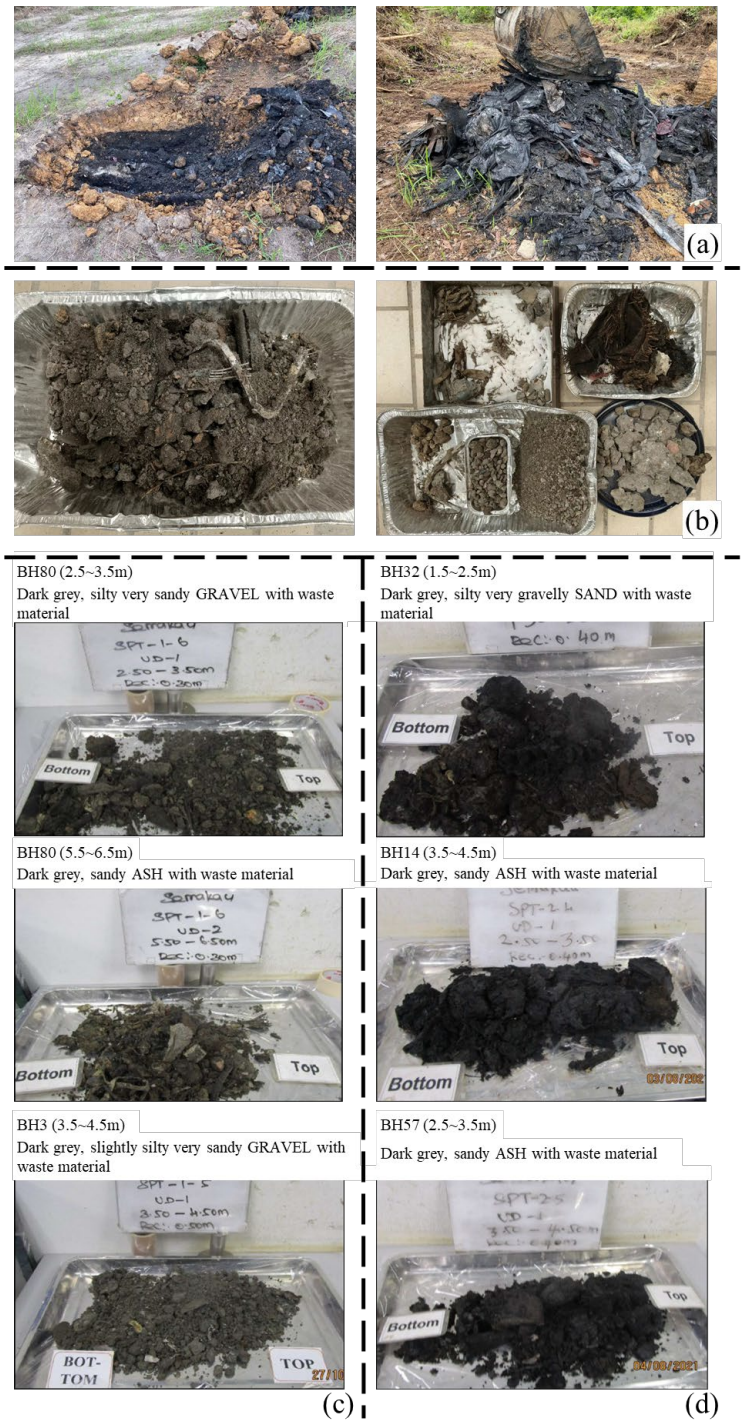


353

354 **Fig. 4.** Underground information obtained from boreholes and water standpipes: (a) waste depth;

355 (b) thickness of waste and groundwater level (mSHD).

356

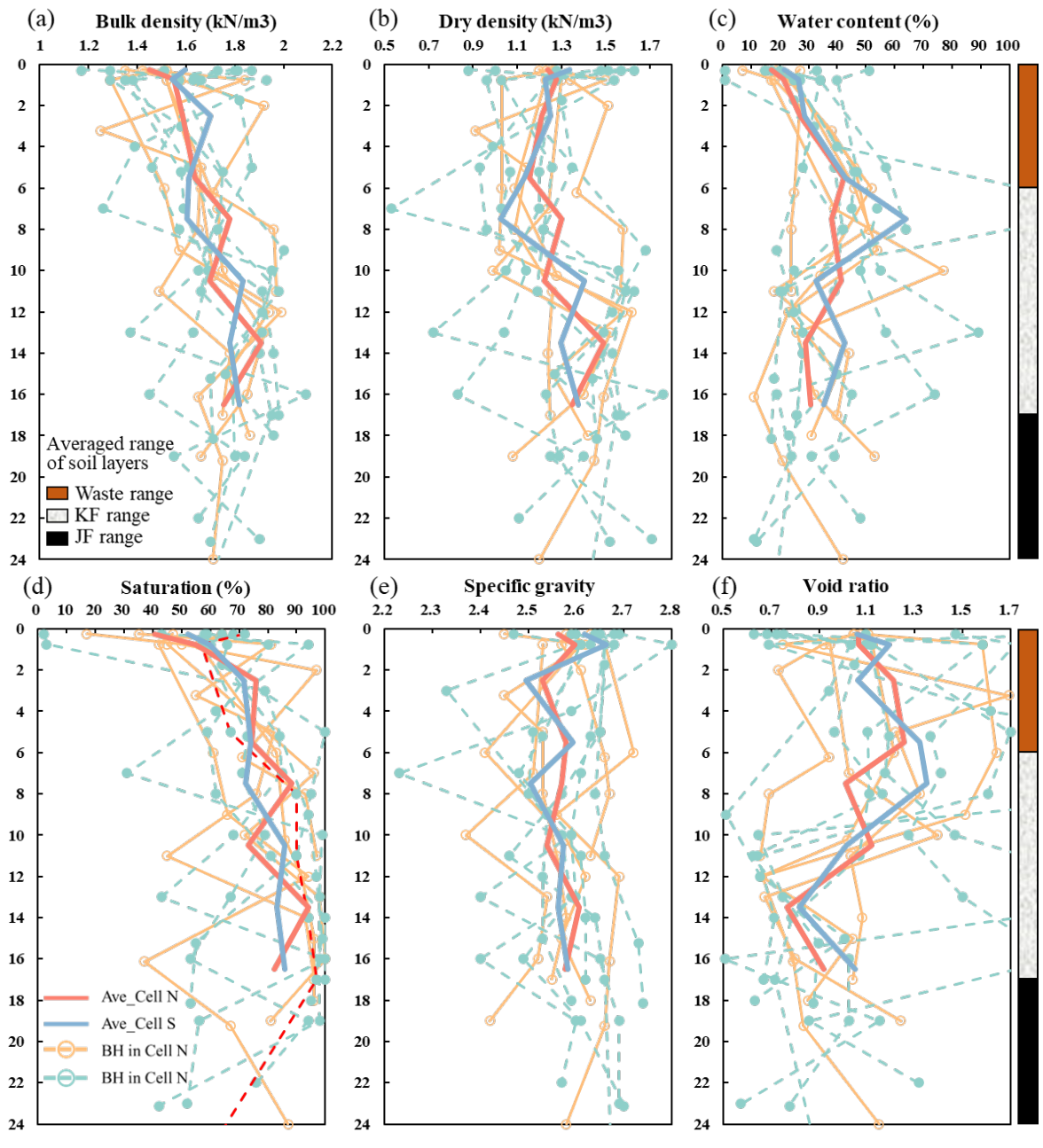


357

358 **Fig. 5.** Photos of retrieved waste samples: (a) as-excavated samples; (b) oven-dried and sieved

359 samples; (c) borehole samples from Cell N; (d) borehole samples from Cell S.

360



361

362 **Fig. 6.** Geotechnical properties of the waste retrieved from different depths: (a) bulk density; (b)

363 dry density; (c) water content; (d) saturation degree; (e) specific gravity; (f) void ratio.

364

365

366 **3.2 Geophysical investigation and waste distribution analysis**

367 To understand the waste distribution within the landfill, geophysical test results were inverted to
368 obtain optimal results (Fig. 7). A comparison with BH and CPT data reveals a V_s profile increasing
369 from 100 to 180 m/s, consistent with established ranges for landfill wastes (Greenwood et al., 2015;
370 Ramaiah et al., 2016; Zekkos et al., 2014) and reaching 220 m/s at the JF interface. Resistivity
371 (Res) serves as a valuable parameter for mapping waste distribution (Samouëlian et al., 2005).
372 Although previous studies highlighted the influence of water level on ERT results (Hu et al., 2019),
373 the impact on this study is limited. This is supported by the absence of significant resistivity
374 changes near the water table in Fig. 7. The high moisture retention of the waste, coupled with the
375 landfill's abundant rainfall and shallow water level, results in elevated water content in the vadose
376 zone above the water level (Fig. 6c). The Res ranged from 9 to 40 Ω·m in the waste layer, which
377 was higher than the saturated clay layer underneath (Fig. 7). The decrease of Res from BH80 to
378 BH18 to BH13 was correlated with increased water content observed in these BHs, validating this
379 trend. While clay typically exhibits higher IP compared to sand, Fig. 7 indicates higher IP in the
380 waste layer comparing with the underlying clay. Surface clay near the waste also shows elevated
381 IP, possibly due to heavy metal leaching from rainfall and groundwater infiltration, or inherent
382 differences between clay layers.
383
384 The integration of geophysical inversion results allowed to generate the 3D model and fence plots
385 shown in Fig. 8. Within Cell S, the central waste layer exhibits higher Vs, indicative of greater
386 strength. Shallow wastes in Cell N generally shows higher Res compared to Cell S, likely due to
387 a higher presence of non-conductive materials such as demolition waste and plastics, along with
388 lower water content. Additionally, the internal road area between Cell N and Cell S has high Res

values due to the low void ratio in this compacted area. Res analysis effectively delineates the internal road coverage, thereby enhancing overall estimates of waste volume. In contrast, Cell S exhibits a stronger IP response, suggesting a higher organic content (Aristodemou and Thomas-Betts, 2000; Leroux et al., 2010). Flores-Orozco et al. (2020) noted that landfills with active biodegradation processes typically exhibit pronounced IP responses.

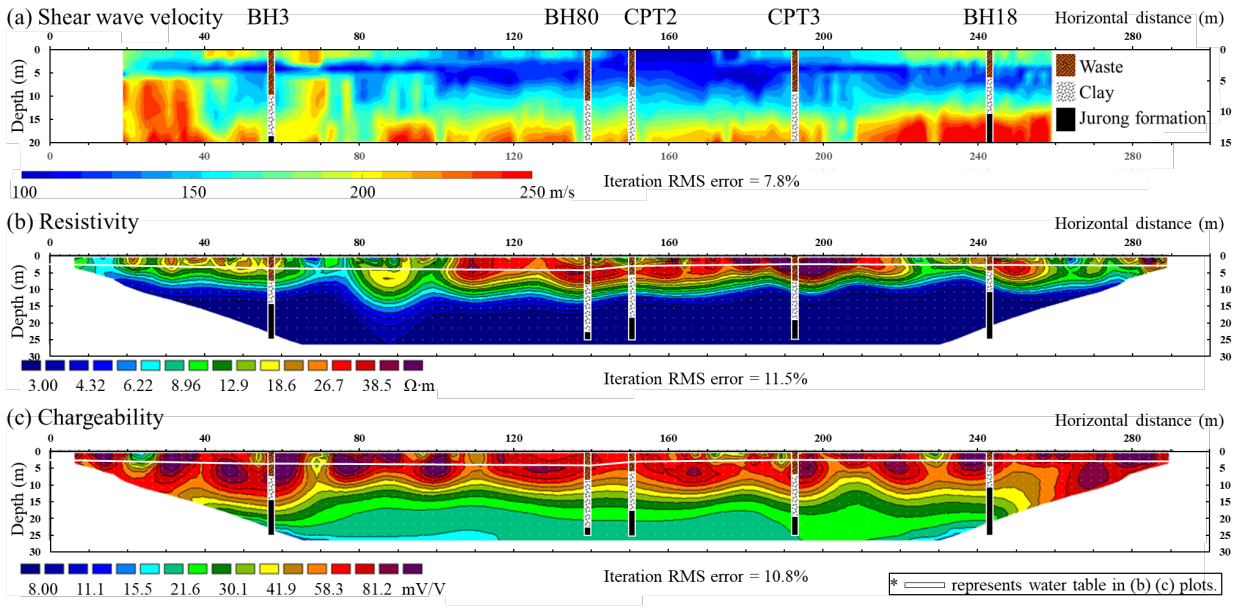


Fig. 7. 2D inversion results of the Cell S A1-G1 cross-section: (a) V_s plot based on MASW and MAM inversion results; (b) Res plot based on ERT inversion results; (c) IP plot based on IP inversion results.

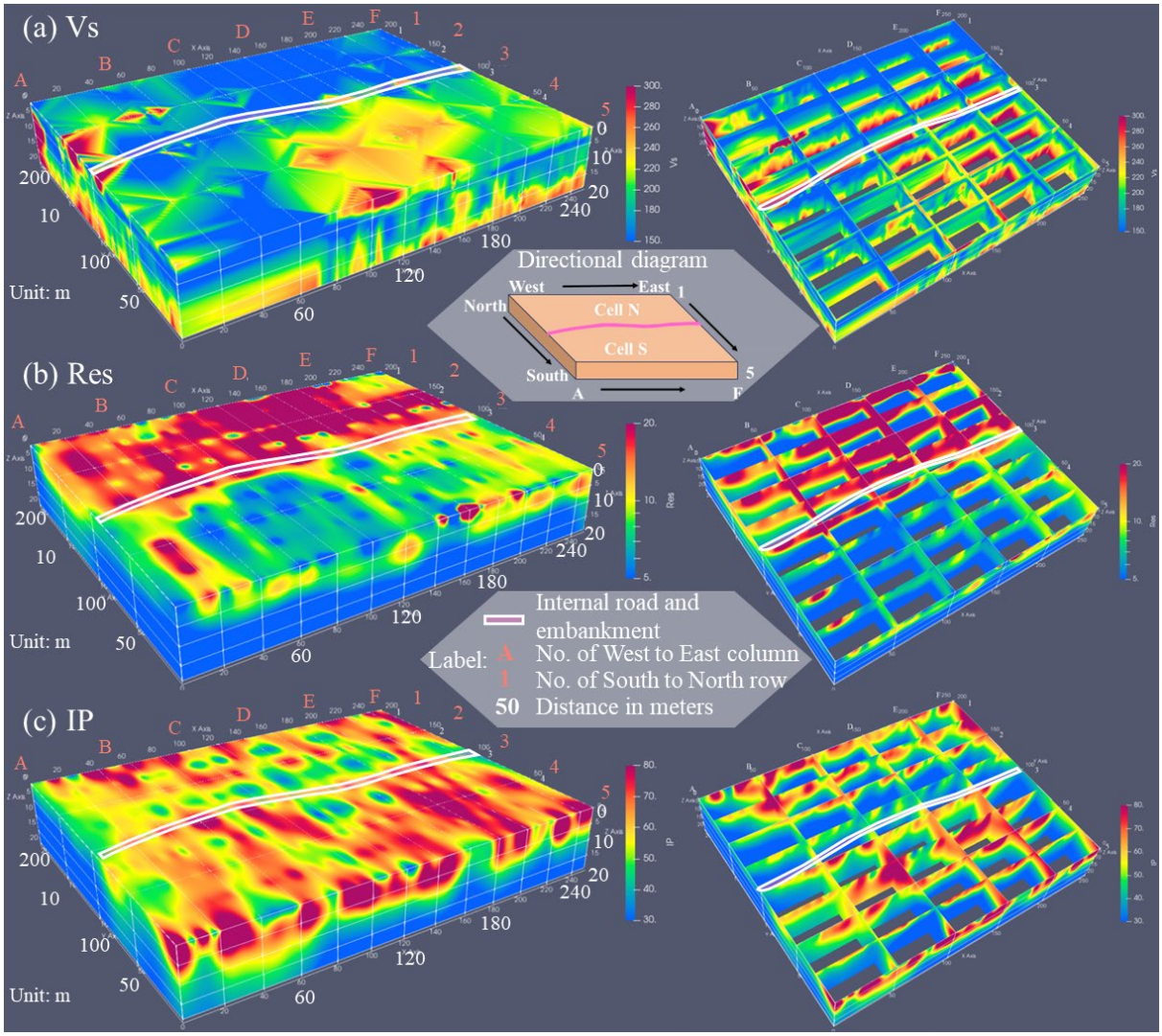


Fig. 8. 3D inversion results of Cell N and Cell S: (a) V_s profile; (b) Res profile; (c) IP profile.

3.3 Quantitative analysis and clustering of geophysical parameter

In addition to qualitative analysis of the geophysical model, accurate delineation of the waste layer and variations in the properties across different areas is essential. Three geophysical parameters, namely V_s, Res, and IP, were standardized by using 10^{th} and 90^{th} percentiles as 0 and 1 namely, to eliminate the influence of different units and numerical orders. These parameters were treated equally during the KMC process, converging based on SSE across multiple iterations. Considering

comparisons with borelogs and CPT records, KMC classified the survey area into six clusters (C0 to C5), detailed in Fig. 9. Clusters C0 to C2 represent deeper sections, while C3 to C5 are shallower. The total surveyed volume of 1,187,500 m^3 covered a space of 250 × 250 × 19 m, with C2 comprising the largest share at 22.4%.

Fig. 10a presents statistical analyses of these clusters, using box plots to depict the mean, median, 10^{th}, 25^{th}, 75^{th}, and 90^{th} percentiles of the V_s, Res, IP, and depth for each category. Across C0 to C5, V_s generally increases with depth, reflecting the effect of longer consolidation periods and greater overburden stress from upper layers, consistent with findings by Sahadewa et al. (2014a). Conversely, Res and IP values decrease gradually, primarily due to changes in moisture content and leachate flows. C4 shows some deviation, likely due to the inclusion of surface waste areas like internal roads with higher Res and V_s, influencing depth ranges. This deviation in IP may stem from compacted natural clay within internal roads. Although the clustering did not directly identify internal roads, it effectively separated them from waste areas, aiding accurate volume estimation. The 3D geophysical space plot shown in Fig. 10b also demonstrates the discriminative capabilities of the three geophysical parameters for natural clay and waste materials, in which C0, C4, C5 can be distinguished with outstanding V_s, IP and Res respectively.

Table 5 confirms geophysical estimates align closely with in-situ measurements, validating clustering accuracy, while Fig. 10b illustrates the discriminative power of V_s, Res, and IP between natural clay and waste materials, capturing variations within the waste layer.

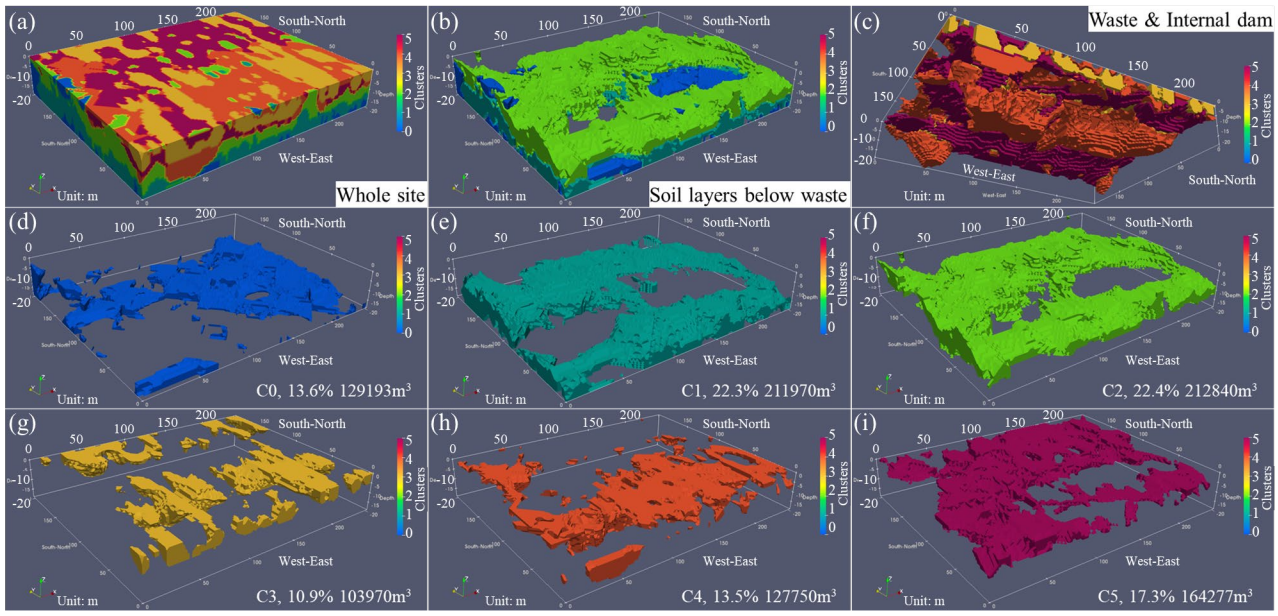


Fig 9. Waste stratification results using the K-means clustering method: (a) whole investigated zone; (b) soil layers below wastes; (c) waste layers and the internal dam; (d) C0 weathered rock layer in JF; (e) C1 bottom stiff clay layer in KF; (f) C2 shallow clay layer in KF; (g) high IP waste layer; (h) stiff waste layer; (i) high res waste layer.

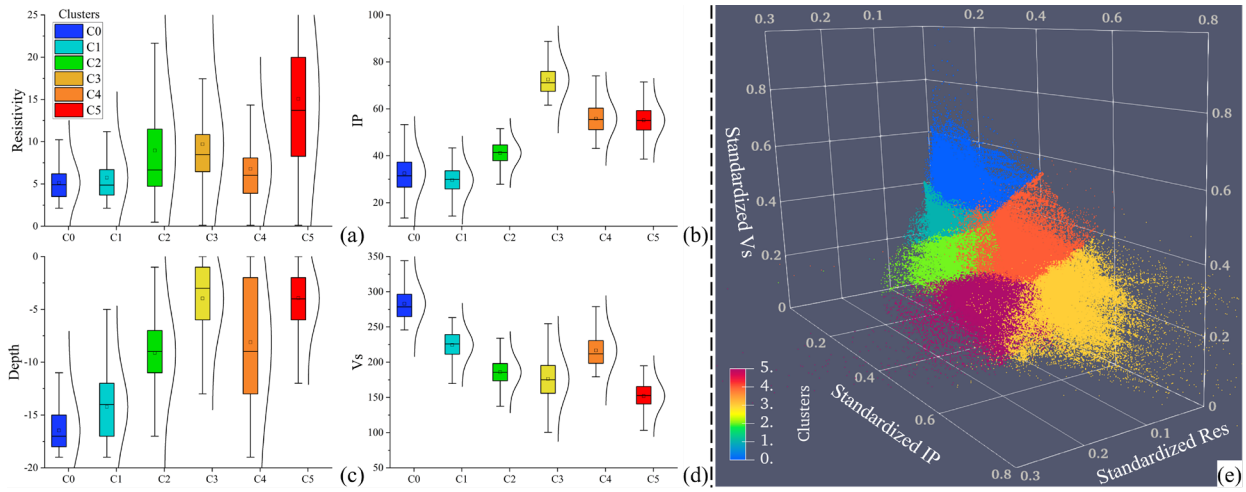


Fig 10. Statistical analyses of the K-means clustering results of Cell N and Cell S for (a) Res; (b) IP; (c) depth; (d) V_s; and (e) distribution of all the geophysical measurements in 3D space.

Table 5. Comparison of the waste depths determined by geotechnical investigation and geophysical clustering and estimation.

BH/CPT		BH or CPT measured waste depth	Geophysical estimated waste depth
within survey scope	BH14	8.5	9.0
	BH56	10.0	8.5
	BH32	7.5	6.0
	BH93	7.5	8.0
	CPT1	6.2	6.0
	CPT2	6.5	11.0
	CPT3*	>6*	11.0

Note: * CPT3 was terminated at 6 m depth as a stiff waste block was encountered.

Based on the clustering results and comprehensive geotechnical and geochemical analysis, Table 6 classified the differences in properties across different strata. C0 corresponds to the distribution range of the JF, with greater depth and significantly higher V_s. C1 represents the deeper layer of the KF. This layer is not affected by leachate, hence exhibiting lower IP, and due to its greater depth, it undergoes more complete consolidation, resulting in higher V_s. C2 represents the shallower layer of the KF, with a relatively higher IP compared to C1 but much lower than the shallower waste layer. This may be attributed to leachate intrusion into the clay adjacent to the waste layer or mixed regions near the waste-clay interface, influencing overall statistical values relative to C1. C3 represents the deepest layer of wastes, with a lower Res relative to C5, consistent with its predominantly sub-water-table conditions. Portions of C4, found between y=80-90 m, include internal roads and artificial dams below, while the remaining distributions of C4 in both cells mainly reside in the shallow layer with higher resistivity. C5 is characterized by shallow burial depth, resulting in weaker soil layers with lower V_s and the highest Res. Overall, the waste

455 layer comprises 42% (C3+C4+C5) of the survey area. Considering Cell N and Cell S cover 0.25
456 km^2, with an average waste density of approximately 1,600 kg/m^3 and 4% metal content, it is
457 estimated that these cells contain a total of 653,000 m^3 of waste materials, including about 3.66
458 tonnes of recoverable metals.
459
460 This study utilizes the offshore landfill as a case study site to demonstrate the application of
461 machine learning-enhanced multi-geophysical investigation methods. Despite numerous
462 geophysical investigations on landfills, there are great disparities in reported results. For instance,
463 Ustra and Elis (2018) reported Res ranging between 2-100 Ω·m in 4 landfills in Brazil, likely
464 influenced by climatic variations and waste composition differences across countries. Singapore's
465 tropical rainforest climate, characterized by abundant rainfall and high temperatures, contrasts with
466 many Northern Hemisphere climates. The composition of solid wastes in Singapore differs
467 significantly from the global average, with higher metal content (19% vs 4%) and lower
468 proportions of food and green waste (14% vs 44%). (NEA, 2023). Therefore, site-specific data
469 collection and pre-investigation are crucial. These efforts not only optimize geophysical site
470 investigation planning but also enhance stratification interpretation.
471
472 The geophysical and clustering results of this study contribute to environmentally sound waste
473 management by (1) promptly detecting and addressing potential leachate leaks through continuous
474 on-site monitoring based on electrical parameters in Table 6; (2) optimizing excavation strategies
475 by mapping compacted zones in C4, thus improving efficiency and cost-effectiveness; and (3)
476 estimating waste volume and recoverable metals using clustering results, facilitating recycling and
477 reuse planning.

Table 6. Descriptions of the waste and soil clusters and their corresponding geophysical parameter ranges

Material type	Cluster	Res value (Ω•m)	IP value (mV/V)	V_s value (m/s)	Description
Jurong formation	C0	5.1 (2.7-7.5)	32.5 (24.0-43.0)	283 (268-316)	14-19m Weathered rock layer in Jurong formation
Kallang formation	C1	5.7 (3.1-9.5)	29.7 (22.0-37.0)	225 (199-247)	10-18m Well-consolidated stiff clay layer
Kallang formation	C2	9.0 (3.6-18.1)	41.2 (35.2-47.1)	186 (163-208)	5-14m Consolidated seabed surface clay in contact with wastes, possibly with leachate intrusion
Waste materials & Compacted soil	C3	9.7 (5.0-16.5)	72.5 (65.2-81.5)	176 (142-211)	0-8m Bio-active areas with higher organic content. High IP might be primarily attributed to the presence of high organic matter components, characterized by their high surface area and surface charge.
	C4	6.8 (3.0-11.3)	55.8 (47.9-63.8)	217 (190-248)	1-16m Stiff wastes, with more particulate matters and higher consolidation level; Contaminated compacted fill soil in the embankment between Cell N and Cell S
	C5	15.1 (6.5-25.3)	55.1 (48.0-62.5)	152 (127-175)	1-7m Dry and soft waste materials at surface

4 Conclusions

This study represents a pioneering effort in offshore landfill characterization. The challenge of low electrical resistivity (Res) in marine clay layers hindered leachate plume identification using conventional methods. However, IP testing successfully identified leachate-intruded areas in clay layers exhibiting higher IP, demonstrating a novel application in offshore environments. By

integrating multiple geophysical methods, this study achieves a comprehensive assessment of landfill sites, heterogeneous areas, and leak detections. ERT accurately delineates waste boundaries due to significant Res differences between waste and seabed clay layers. High IP zones identified areas rich in recoverable metals or ongoing biodegradation. V_s distribution not only located embankment ranges and areas with high amounts of construction wastes and cemented ashes, but also allowed to evaluate the consolidation level of waste materials, which are crucial for effective waste management strategies. The application of unsupervised machine learning methods in clustering results eliminated subjective biases, establishing clear delineation standards and providing transparent descriptions of site geophysical characteristics. Trustworthy estimates of total waste volume and recoverable metal quantities derived from clustering results enhance landfill management practices. Validation of geophysical findings through integration with geotechnical and geochemical data enhanced the credibility and interpretability of machine learning stratification results. The stratification model can support continuous site monitoring via geophysical surveys, enabling timely detection and remediation of potential leachate leaks, thereby improving overall waste management efficiency and effectiveness. While the innovative approach of this study shows promise for widespread application in landfill investigations, there are still limitations and shortcomings that need to be addressed. These include limited sample data and the need for establishing quantitative relationships between geophysical parameters and waste physicochemical properties. Addressing these gaps through expanded dataset analyses and advanced inversion techniques will be crucial for refining methodologies and advancing understanding in future research.

Abbreviation

APHA	American Public Health Association
bgl	below the groundwater level
BH	Borehole
CPT	Cone penetration test
EM	Electrical magnetics
EPA	Environmental Protection Agency, USA
ERT	Electrical resistivity tomography
EV BH	Environmental borehole
f_s	Sleeve friction
GMM	Gaussian mixture model
GPR	Ground penetrating radar
G_s	Specific gravity
IBA	Incineration bottom ash
IFA	Incineration fly ash, incineration fly ash
NIW	Non-incinerable waste
IP	Induced polarization, also represents chargeability
IV	Intervention values
JF	Jurong Formation
KF	Kallang Formation
KMC	K-means clustering
MAM	Microtremor array method
MASW	Multi-channel analysis of surface wave

N	Blow number in SPT
NS	North to South
q_t	Tip resistance
Res	Resistivity
SASW	Spectral Analysis of Surface Waves
SDG 12	Sustainable Development Goal 12
SPT	Standard penetration test
SSE	Sum of standard error
u_0	Water pressure
V_s	Shear wave velocity
WE	West to east

Acknowledgement

This research/project is supported by the National Research Foundation, Singapore, and the National Environment Agency, Singapore under its Closing the Waste Loop Funding Initiative (Award No. USS-IF-2021-4). Any opinions, findings and conclusions or recommendations expressed in this material are those of the author(s) and do not reflect the views of National Research Foundation, Singapore, and the National Environment Agency, Singapore.

References

Abdulsamad, F., Florsch, N., Schmutz, M., Camerlynck, C., 2016. Assessing the high frequency behavior of non-polarizable electrodes for spectral induced polarization measurements. Journal of Applied Geophysics 135, 449-455. https://doi.org/10.1016/j.jappgeo.2016.01.001

555 Abreu, A.E., Gandolfo, O.C., Vilar, O.M., 2016. Characterizing a Brazilian sanitary landfill using
556 geophysical seismic techniques. Waste Management 53, 116-127.
557 http://doi.org/10.1016/j.wasman.2016.03.048
558 Aki, K., 1957. Space and time spectra of stationary stochastic waves, with special reference to
559 microtremors. Bulletin of the Earthquake Research Institute 35, 415-456.
560 APHA, 2017a. Method 3112B. Metals by cold-vapor atomic absorption spectrometry. Standard
561 Methods for the Examination of Water and Wastewater. American Public Health Association,
562 Washington DC. https://law.resource.org/pub/us/cfr/ibr/002/apha.method.3112.1992.pdf
563 APHA, 2017b. Method 3120B. Inductively Coupled Plasma (ICP) method. Standard Methods for
564 the Examination of Water and Wastewater. American Public Health Association,
565 Washington DC. https://law.resource.org/pub/us/cfr/ibr/002/apha.method.3120.1992.pdf
566 APHA, 2017c. Method 3125B. Metals by inductively coupled plasma-mass spectrometry.
567 Standard Methods for the Examination of Water and Wastewater. American Public Health
568 Association, Washington DC. https://doi.org/10.2105/SMWW.2882.048
569 Aristodemou, E., Thomas-Betts, A., 2000. DC resistivity and induced polarisation investigations
570 at a waste disposal site and its environments. Journal of Applied Geophysics 44(2-3), 275-
571 302. https://doi.org/10.1016/S0926-9851(99)00022-1
572 ASTM, 2016. ASTM D3441-16, Standard Test Method for Mechanical Cone Penetration Testing
573 of Soils. https://doi.org/10.1520/D3441-16
574 Aziz, H.A., Ghazali, M.F., Hung, Y.-T., Wang, L.K., 2017. Toxicity, source, and control of barium
575 in the environment, Handbook of Advanced Industrial and Hazardous Wastes Management.
576 CRC Press, pp. 463-482.

577 Bholowalia, P., Kumar, A., 2014. EBK-means: A clustering technique based on elbow method and
578 k-means in WSN. International Journal of Computer Applications 105(9).
579 Carpenter, P.J., Reddy, K.R., Thompson, M.D., 2013. Seismic imaging of a leachate-recirculation
580 landfill: spatial changes in dynamic properties of municipal solid waste. Journal of
581 Hazardous, Toxic, and Radioactive Waste 17(4), 331-341.
582 https://doi.org/10.1061/(ASCE)HZ.2153-5515.0000175
583 Chambers, J.E., Kuras, O., Meldrum, P.I., Ogilvy, R.D., Hollands, J., 2006. Electrical resistivity
584 tomography applied to geologic, hydrogeologic, and engineering investigations at a former
585 waste-disposal site. Geophysics 71(6), B231-B239.
586 https://library.seg.org/doi/abs/10.1190/1.2360184#
587 Circular, S.R., 2013. Rijkswaterstaat, Ministry of Infrastructure and the Environment, Netherlands.
588 Clément, R., Descloitres, M., Günther, T., Oxarango, L., Morra, C., Laurent, J.-P., Gourc, J.-P.,
589 2010. Improvement of electrical resistivity tomography for leachate injection monitoring.
590 Waste management 30(3), 452-464. https://doi.org/10.1016/j.wasman.2009.10.002
591 Cuevas, J., Ruiz, A.I., de Soto, I.S., Sevilla, T., Procopio, J.R., Da Silva, P., Gismera, M.J.,
592 Regadío, M., Jiménez, N.S., Rastrero, M.R., 2012. The performance of natural clay as a
593 barrier to the diffusion of municipal solid waste landfill leachates. Journal of Environmental
594 Management 95, S175-S181. https://doi.org/10.1016/j.jenvman.2011.02.014
595 Di Maio, R., Fais, S., Ligas, P., Piegari, E., Raga, R., Cossu, R., 2018. 3D geophysical imaging
596 for site-specific characterization plan of an old landfill. Waste Management 76, 629-642.
597 10.1016/j.wasman.2018.03.004

598 Dumont, G., Robert, T., Marck, N., Nguyen, F., 2017. Assessment of multiple geophysical
599 techniques for the characterization of municipal waste deposit sites. Journal of Applied
600 Geophysics 145, 74-83. https://doi.org/10.1016/j.jappgeo.2017.07.013
601 EPA, 2007. Method 3051A. Microwave Assisted Acid Digestion of Sediments, Sludges, Soils,
602 and Oils. U.S. Environmental Protection Agency, Washington DC.
603 http://refhub.elsevier.com/S0883-2927(16)30418-8/sref42
604 EPA, 2014. Method 6010D. Inductively Coupled Plasma-atomic Emission Spectrometry. U.S.
605 Environmental Protection Agency, Washington DC. http://refhub.elsevier.com/S0883-
606 2927(16)30418-8/sref45
607 Fei, X., Fang, M., Wang, Y., 2021. Climate change affects land-disposed waste. Nature Climate
608 Change 11(12), 1004-1005. https://doi.org/10.1038/s41558-021-01220-5
609 Fei, X., Guo, Y., Wang, Y., Fang, M., Yin, K., He, H., 2022. The long-term fates of land-disposed
610 plastic waste. Nature Reviews Earth & Environment 3(11), 733-735.
611 https://doi.org/10.1038/s43017-022-00354-0
612 Fei, X., Zekkos, D., 2018. Coupled experimental assessment of physico-biochemical
613 characteristics of municipal solid waste undergoing enhanced biodegradation. Géotechnique
614 68(12), 1031-1043. https://doi.org/10.1680/jgeot.16.P.253
615 Fei, X., Zekkos, D., Raskin, L., 2016. Quantification of parameters influencing methane generation
616 due to biodegradation of municipal solid waste in landfills and laboratory experiments.
617 Waste management 55, 276-287. https://doi.org/10.1016/j.wasman.2015.10.015
618 Gabarrón, M., Martínez-Pagán, P., Martínez-Segura, M.A., Bueso, M.C., Martínez-Martínez, S.,
619 Faz, Á., Acosta, J.A., 2020. Electrical resistivity tomography as a support tool for

physicochemical properties assessment of near-surface waste materials in a mining tailing pond (El Gorguel, SE Spain). Minerals 10(6), 559. https://doi.org/10.3390/min10060559

Greenwood, W., Zekkos, D., Sahadewa, A., 2015. Spatial Variation of Shear Wave Velocity of Waste Materials from Surface Wave Measurements. Journal of Environmental and Engineering Geophysics 20(4), 287-301. http://doi.org/10.2113/jeeg20.4.287

He, H., Fei, X., 2020. Scaling up laboratory column testing results to predict coupled methane generation and biological settlement in full-scale municipal solid waste landfills. Waste Management 115, 25-35. https://doi.org/10.1016/j.wasman.2020.07.018

He, H., Gao, X., Fei, X., 2023. Generation and management of municipal solid waste in top metropolitans of China: A comparison with Singapore. Circular Economy 2(2), 100041.

Hu, J., Wu, X.W., Ke, H., Xu, X.B., Lan, J.W., Zhan, L.T., 2019. Application of electrical resistivity tomography to monitor the dewatering of vertical and horizontal wells in municipal solid waste landfills. Engineering geology 254, 1-12. https://doi.org/10.1016/j.enggeo.2019.03.021

ISWA, I.S.W.A., 2024. Global waste management outlook 2024: beyond an age of waste, turning rubbish into a resource.

Jacobs, J., 2018. Europe's half a million landfill sites potentially worth a fortune, Financial Times.

Jones, P.T., Geysen, D., Tielemans, Y., Van Passel, S., Pontikes, Y., Blanpain, B., Quaghebeur, M., Hoekstra, N., 2013. Enhanced Landfill Mining in view of multiple resource recovery: a critical review. Journal of Cleaner Production 55, 45-55. https://doi.org/10.1016/j.jclepro.2012.05.021

Kaza, S., Yao, L., Bhada-Tata, P., Van Woerden, F., 2018. What a waste 2.0: a global snapshot of solid waste management to 2050. World Bank Publications.

643 Kou, H.-l., Chu, J., Guo, W., Zhang, M.-y., 2016. Field study of residual forces developed in pre-
644 stressed high-strength concrete (PHC) pipe piles. Canadian Geotechnical Journal 53(4), 696-
645 707. https://doi.org/10.1139/cgj-2015-0177
646 Leroux, V., Dahlin, T., Rosqvist, H., 2010. Time-domain IP and resistivity sections measured at
647 four landfills with different contents, Near Surface 2010-16th EAGE European Meeting of
648 Environmental and Engineering Geophysics. European Association of Geoscientists &
649 Engineers, pp. cp-164-00086. https://doi.org/10.3997/2214-4609.20144851
650 Lloyd, S., 1982. Least squares quantization in PCM. IEEE transactions on information theory
651 28(2), 129-137.
652 Loke, M., Chambers, J., Rucker, D., Kuras, O., Wilkinson, P., 2013. Recent developments in the
653 direct-current geoelectrical imaging method. Journal of applied geophysics 95, 135-156.
654 https://doi.org/10.1016/j.jappgeo.2013.02.017
655 Loke, M.H., Barker, R.D., 1996. Rapid least - squares inversion of apparent resistivity
656 pseudosections by a quasi - Newton method1. Geophysical prospecting 44(1), 131-152.
657 https://doi.org/10.1111/j.1365-2478.1996.tb00142.x
658 M.H.Loke, 2022. Tutorial : 2-D and 3-D electrical imaging surveys. http://www.geotomosoft.com/.
659 (Accessed 3rd May 2022).
660 Manrique, I.I., Hermans, T., Caterina, D., Jougnot, D., Mignon, B., Masse, A., Nguyen, F., 2024.
661 Integrated methodology to link geochemical and geophysical-lab data in a geophysical
662 investigation of a slag heap for resource quantification. Journal of Environmental
663 Management 349, 119366. https://doi.org/10.1016/j.jenvman.2023.119366
664 NEA, 2023. Waste Statistics and Overall Recycling. https://www.nea.gov.sg/our-services/waste-
665 management/waste-statistics-and-overall-recycling. (Accessed 15 April 2024).

Olafsdottir, E.A., Erlingsson, S., Bessason, B., 2018. Tool for analysis of multichannel analysis of surface waves (MASW) field data and evaluation of shear wave velocity profiles of soils. Canadian Geotechnical Journal 55(2), 217-233. https://doi.org/10.1139/cgj-2016-0302

Oldenburg, D.W., Li, Y., 1994. Inversion of induced polarization data. Geophysics 59(9), 1327-1341. https://doi.org/10.1190/1.1443692

Pazzi, V., Morelli, S., Fanti, R., 2019. A review of the advantages and limitations of geophysical investigations in landslide studies. International Journal of Geophysics 2019. https://doi.org/10.1155/2019/2983087

Pi, X., Fei, X., Wang, Y., Sun, X., Guo, Y., 2023. Global void ratio of municipal solid waste for compression indices estimation. Waste Management 160, 69-79. https://doi.org/10.1016/j.wasman.2023.02.003

Pomposiello, C., Dapeña, C., Favetto, A., Boujon, P., 2012. Application of geophysical methods to waste disposal studies. Municipal and Industrial Waste Disposal, 3-26. http://doi.org/10.5772/29615

Ramaiah, B.J., Ramana, G.V., Kavazanjian, E., Matasovic, N., Bansal, B.K., 2016. Empirical Model for Shear Wave Velocity of Municipal Solid Waste In Situ. Journal of Geotechnical and Geoenvironmental Engineering 142(1). http://doi.org/10.1061/(asce)gt.1943-5606.0001389

Sahadewa, A., Zekkos, D., Fei, X., Li, J., Zhao, X., 2014a. Recurring shear wave velocity measurements at the Smiths Creek bioreactor landfill, Geo-Congress 2014: Geo-characterization and Modeling for Sustainability. pp. 2072-2081. https://doi.org/10.1061/9780784413272.202

688 Sahadewa, A., Zekkos, D., Woods, R.D., Stokoe II, K.H., Matasovic, N., 2014b. In-situ assessment
689 of the dynamic properties of municipal solid waste at a landfill in Texas. Soil Dynamics and
690 Earthquake Engineering 65, 303-313. https://doi.org/10.1016/j.soildyn.2014.04.004
691 Samouëlian, A., Cousin, I., Tabbagh, A., Bruand, A., Richard, G., 2005. Electrical resistivity
692 survey in soil science: a review. Soil and Tillage research 83(2), 173-193.
693 https://doi.org/10.1016/j.still.2004.10.004
694 Soupios, P., Papadopoulos, N., Papadopoulos, I., Kouli, M., Vallianatos, F., Sarris, A., Manios, T.,
695 2007. Application of integrated methods in mapping waste disposal areas. Environmental
696 geology 53(3), 661-675. https://doi.org/10.1007/s00254-007-0681-2
697 Steiner, M., Katona, T., Fellner, J., Orozco, A.F., 2022. Quantitative water content estimation in
698 landfills through joint inversion of seismic refraction and electrical resistivity data
699 considering surface conduction. Waste Management 149, 21-32.
700 https://doi.org/10.1016/j.wasman.2022.05.020
701 Sumner, J.S., 2012. Principles of induced polarization for geophysical exploration. Elsevier.
702 Titov, K., Komarov, V., Tarasov, V., Levitski, A., 2002. Theoretical and experimental study of
703 time domain-induced polarization in water-saturated sands. Journal of applied geophysics
704 50(4), 417-433. https://doi.org/10.1016/S0926-9851(02)00168-4
705 Ustra, A., Elis, V.R., 2018. Resistivity and induced polarization application for urban waste
706 disposal site studies, Applied Geophysics with Case Studies on Environmental, Exploration
707 and Engineering Geophysics. IntechOpen. http://doi.org/10.5772/intechopen.81225
708 Vaverková, M.D., 2019. Landfill impacts on the environment. Geosciences 9(10), 431.
709 https://doi.org/10.3390/geosciences9100431

Wagland, S.T., Coulon, F., Canopoli, L., 2019. Developing the case for enhanced landfill mining in the UK. https://doi.org/10.31025/2611-4135/2019.13772

Wang, H., Wu, S., Qi, X., Chu, J., 2021. Site characterization of reclaimed lands based on seismic cone penetration test. Engineering Geology 280, 105953. https://doi.org/10.1016/j.enggeo.2020.105953

Wang, J., Zhang, J.-t., Zhu, T., 2024. Two-Sample Test for High-Dimensional Covariance Matrices: a normal-reference approach. Journal of Multivariate Analysis. https://doi.org/10.1016/j.jmva.2024.105354

Wang, Q., Ko, J.H., Liu, F., Xu, Q., 2021. Leaching characteristics of heavy metals in MSW and bottom ash co-disposal landfills. Journal of hazardous materials 416, 126042. https://doi.org/10.1016/j.jhazmat.2021.126042

Wei, W., Liu, Q., Zhang, Z., Lisak, G., Yin, K., Fei, X., 2024. Categorization of leaching behaviors of elements from commercially treated incineration bottom ash in Singapore. Waste Management 178, 339-350. https://doi.org/10.1016/j.wasman.2024.02.045

Yin, K., Tong, H.H., Noh, O., Wang, J.-Y., Giannis, A., 2015. Mapping refuse profile in Singapore old dumping ground through electrical resistivity, S-wave velocity and geotechnical monitoring. Bulletin of environmental contamination and toxicology 94, 275-281. https://doi.org/10.1007/s00128-014-1427-y

Zekkos, D., Bray, J.D., Riemer, M.F., 2008. Shear modulus and material damping of municipal solid waste based on large-scale cyclic triaxial testing. Canadian Geotechnical Journal 45(1), 45-58. https://doi.org/10.1139/T07-069

731 Zekkos, D., Kabalan, M., Syal, S.M., Hambright, M., Sahadewa, A., 2013. Geotechnical
732 characterization of a Municipal Solid Waste Incineration Ash from a Michigan monofill.
733 Waste Management 33(6), 1442-1450. http://doi.org/10.1016/j.wasman.2013.02.009
734 Zekkos, D., Sahadewa, A., Woods, R.D., Stokoe, K.H., 2014. Development of Model for Shear-
735 Wave Velocity of Municipal Solid Waste. Journal of Geotechnical and Geoenvironmental
736 Engineering 140(3). https://doi.org/10.1061/(ASCE)GT.1943-5606.0001017
737 Zhang, Z., Fei, X., Wu, W., 2023. Monotonic and cyclic shear behaviors of incineration bottom
738 ash under constant volume condition, 9th International Congress on Environmental
739 Geotechnics. Chania, Greece. https://doi.org/10.53243/ICEG2023-431
740 Zhang, Z., Wang, J., Li, J., Wang, Y., Yin, K., Fei, X., 2024. Impacts of regional socioeconomic
741 statuses and global events on solid waste research reflected in six waste-focused journals.
742 Waste Management 182, 113-123.
743



https://dspace.org/

Comprehensive geophysical, geotechnical, and geochemical assessments of an offshore landfill in Singapore

Zhang, Zhibo; Yuan, Ziwen; Hu, Lei; Coulon, Frederic; Liu, Huaxin ...

2024-12-05
Elsevier
https://doi.org/10.1016/j.jhazmat.2024.135908
Zhang Z, Yuan Z, Hu L, et al., (2024) Comprehensive geophysical, geotechnical, and geochemical assessments of an offshore landfill in Singapore. Journal of Hazardous Materials, Volume 480, December 2024, Article number 135908

Downloaded from a DSpace repository. https://dspace.org/